Electronic cam motion generation with special reference to constrained velocity, acceleration, and jerk

Chung-Shu Liao,[a] Shyr-Long Jeng,[b] Wei-Hua Chieng[a]

[a]Department of Mechanical Engineering, National Chiao-Tung University, 1001 Ta Hsueh Road, Hsinchu, Taiwan 30010, Republic of China
[b]Department of Automation Engineering, Ta Hwa Institute of Technology, 1 Ta-Hwa Road, Chiung-Lin, Hsinchu, Taiwan, Republic of China

Abstract

Electronic cam motion involves velocity tracking control of the master motor and trajectory generation of the slave motor. Special concerns such as the limits of the velocity, acceleration, and jerk are beyond the considerations in the conventional electronic cam motion control. This study proposes the curve-fitting of a Lagrange polynomial to the cam profile, based on trajectory optimization by cubic B-spline interpolation. The proposed algorithms may yield a higher tracking precision than the conventional master-slaves control method does, providing an optimization problem is concerned. The optimization problem contains three dynamic constraints including velocity, acceleration, and jerk of the motor system. © 2004 ISA—The Instrumentation, Systems, and Automation Society.

Keywords: Electronic cam; Tracking control; Trajectory generation; Trajectory optimization; Master-slaves

1. Introduction

In this study, the electronic cam (ECAM) motion is generated in two stages, the first of which is a typical electronic gearing process which is focused on the velocity tracking control of the master motor. Steven [1] specified a tracking control electronic gearing system called an "optimal feedforward tracking controller," concerned primarily with the design of the slave controller. However, he did not consider the output properties of the master motor, including the measurement noise, periodic errors, and external harmonic disturbances. In practice, the measurement noise or the external disturbance must be controlled and eliminated by modeling the disturbances, before applying tracking control to estimate the master position. This paper proposes the use of a disturbance estimator [2] to suppress the external disturbance.

The design of this disturbance estimator is practical and easy to implement.

This approach to obtaining a highly precise estimate of the master position involves Nth-order polynomial tracking. For example, the fifth-order polynomial estimate is more precise than the third-order polynomial estimation by a factor of about 10 000. The advantage of the proposed tracking method is that the low-frequency harmonic disturbances of a loaded master are very precisely estimated. Such nominal harmonic disturbances are observed in many industrial applications [3]. In practice, the frequencies of the external disturbances are expected to be far below the Nyquist frequency [4] of the real-time system.

ECAM motion regulates the slave motion to follow a predetermined trajectory, which is a function of the position of the master axis [5,6]. A cam

trajectory is generally specified by a cam profile table, which lists a set of reciprocal coordinates. Chen [7] applied B-spline [8,9] and polynomial curve-fitting methods to generate a smooth cam profile curve function. Kim and Tsao [10] developed an electrohydraulic servo actuator for use in electronic cam motion generation, and obtained improved performance. However, some original performance limits, including velocity, acceleration, or jerk constraints, must be considered because motors have the lower loaded capacity relative to the hydraulic actuators. For example, for a highly precise machining tool, chattering must be avoided, so jerking in motion must be reduced.

This study proposes an optimization algorithm [11] to prevent extremely high velocities, acceleration, or jerk, yielding smooth motion of the slave motor without loss of precision. The proposed tracking method presented here was experimentally verified using a real-time program to realize the ECAM control system. The master's system uses a disturbance estimator to eliminate external disturbances. This estimator is the prerequisite for the Nth-order polynomial tracking control. Lagrange polynomial [9] curve-fitting, cubic B-spline [9] interpolation and a constrained optimization algorithm are used to determine the position of the slaves. Consequently, a tradeoff may exist between precision and constraints, which are imposed in given order of priority.

2. Prerequisite of electronic cam (ECAM) tracking control

Electronic cam (ECAM) control is a well-known master-slaves system. Fig. 1(a) schematically depicts the mathematical model of the proposed electronic cam system. The variables and symbols in the figure are defined in the following sections. In Fig. 1(a), the motion of the slave motor clearly depends on the estimated slave position command, p_{k+1}, which is generated by cubic B-spline interpolation, combined with an optimization algorithm. Such optimization is performed to meet the demands of limited performance—the constraints of velocity, acceleration, and jerk. The method of cubic B-spline curve-fitting is based on substituting the estimated master position into the cam trajectory. It is established using Lagrange's interpolation formula to generate a Lagrange poly-

nomial curve. However, the predicted master position is estimated by the electronic gearing (E-gearing) process.

2.1. External disturbance estimator

External disturbances (or loads) applied to the master may directly impact the efficiency of E-gearing. Therefore disturbances must be suppressed. A mathematical model of the disturbance estimator, depicted in Fig. 1(a), is used to estimate and suppress the external loads of the master motor. Fig. 1(b) is one practical embodiment for the proposed disturbance suppressed control.

In Fig. 1(b), the external load τ_L is estimated from the input current i_a and the angular velocity ω, where K_a, $\hat{L}_f$, $\hat{R}_f$, $\hat{K}$, $\hat{J}$, and $\hat{B}$ represent the nominal back electromotive force constant, the nominal armature current inductance, the nominal armature current resistance, the nominal torque constant, the nominal moment of inertia, and the nominal damping coefficient of the motor, respectively. Furthermore, V_{ref}, L_f, R_f, K, J, and B represent the reference voltage input, the actual armature current inductance, the actual armature current resistance, the actual (uncertain) torque constant, the actual (uncertain) moment of inertia, and the actual (uncertain) damping coefficient of the motor, respectively. Consider the dynamics of a typical dc motor:

$$\hat{J}\dot{\omega} + \hat{B}\omega + \tau_L = \hat{K} \cdot i_a \Rightarrow \tau_L = \hat{K} \cdot i_a - \hat{J}\dot{\omega} - \hat{B}\omega. \tag{1}$$

According to Fig. 2(a), this estimator cannot be realized because of the differential term ($\hat{J}s$) of angular velocity. The estimator depicted in Fig. 2(a) is also very numerically sensitive to the measurement noise because it yields high gains in the high-frequency field. Accordingly, a first-order low-pass filter is used to estimate the disturbance $\hat{\tau}_L$, as shown in Fig. 2(b), where

$$\hat{\tau}_L = \frac{1}{(\Im s + 1)} \tau_L \tag{2}$$

and

$$\frac{\hat{\tau}_L}{\omega} = \frac{-(\hat{J}s + B)}{\Im s + 1} = -\frac{\hat{J}}{\Im} + \frac{-\hat{B} + \hat{J}/\Im}{\Im s + 1}. \tag{3}$$

Rearranging this external disturbance estimator in Fig. 3 yields no differential term. The estimated
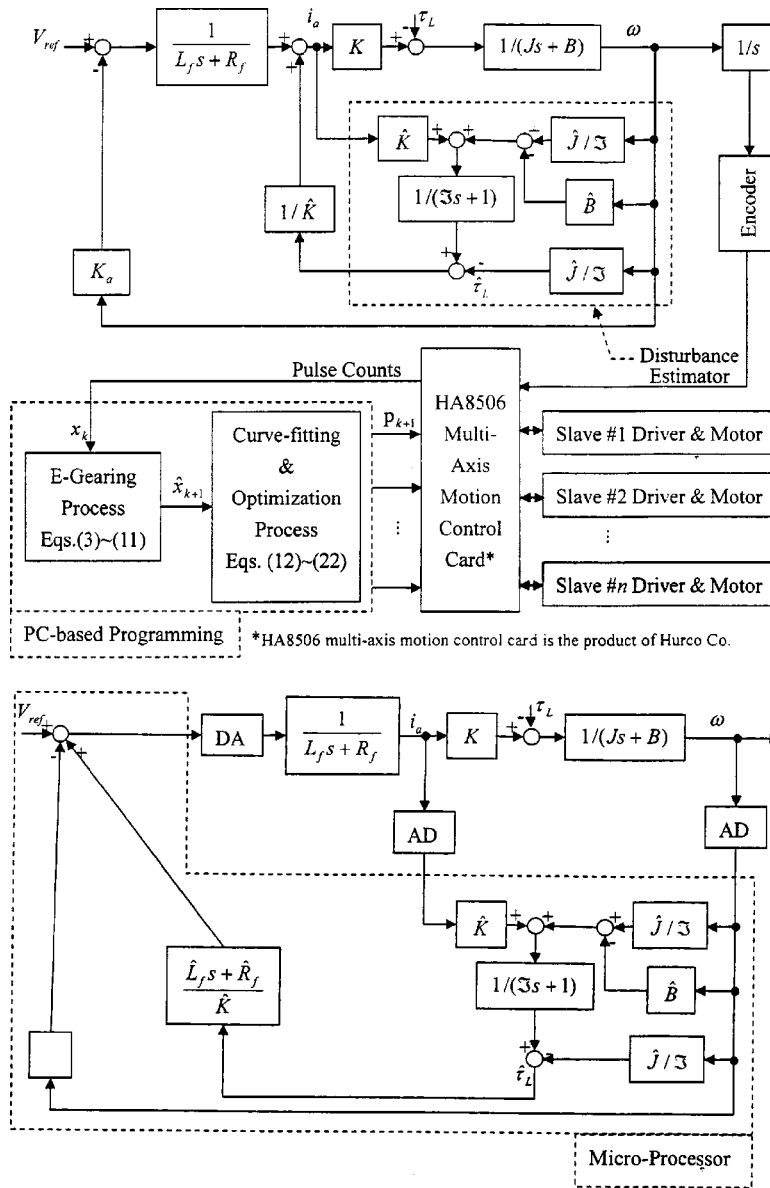
Fig. 1. (a) Mathematical model of the proposed electronic cam system. (b) Block diagram of the proposed disturbance estimator for one practical embodiment.

disturbance ($\hat{\tau}_L$) is then fed back to the current loop, and the external disturbance is suppressed. In practice, due to the current loop's bandwidth being much larger than the speed loop's bandwidth, the electrical dynamic response $[1/(L_f s + R_f)]$ may be ignored from the model of Fig. 1(b).

2.2. Suppressing external disturbance

According to Fig. 3, the pole of the disturbance estimator equals the pole of the low-pass filter,

specified by Eq. (2). Thus the estimated value for low delay time is obtained by reducing the time constant ($\Im$) of the low-pass filter. However, the small time constant trades off the estimated precision and robustness because it suffers more on measurement noise and modeling uncertainty.

Fig. 2(b) is equivalently transformed to Fig. 2(c) to elucidate the effect of the external disturbance (τ_L). According to Fig. 2(c), the effect of τ_L is that of passing τ_L through the filter $\Im s/(\Im s + 1)$. Accordingly, the external disturbance can be suppressed when the disturbance frequency is less
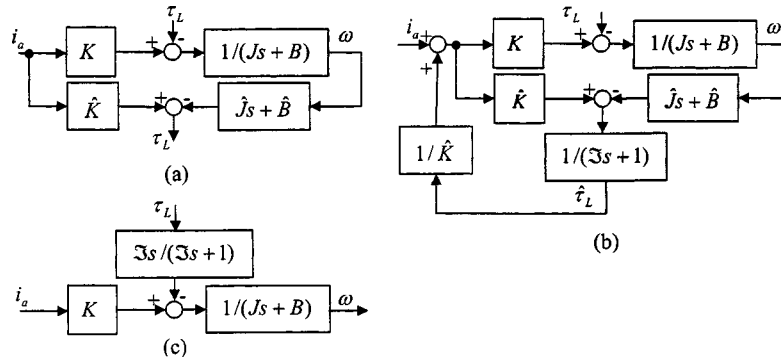
Fig. 2. The estimation of external disturbance.

than $1/\Im$ rad/s. Thus the smaller time constant $\Im$ yields better efficiency for suppressing high-frequency disturbances. However, a tradeoff exists between estimated precision and robustness, as described in the above paragraph.

Due to considerations of robustness, the measurement noise and the modeling uncertainty must also be considered in determining the time constant $\Im$. The Appendix discusses the sensitivities, $S_K^{G_c}$, $S_J^{G_c}$, and $S_B^{G_c}$ to the uncertainties, where $S_K^{G_c}$, $S_J^{G_c}$, and $S_B^{G_c}$ are the sensitivities of the current loop transfer function G_c to the uncertain parameters K, J, and B, respectively. Moreover, the effect of measurement noise is discussed with reference to a numerical simulation in Section 5.1.

3. Electronic gearing (E-gearing) process

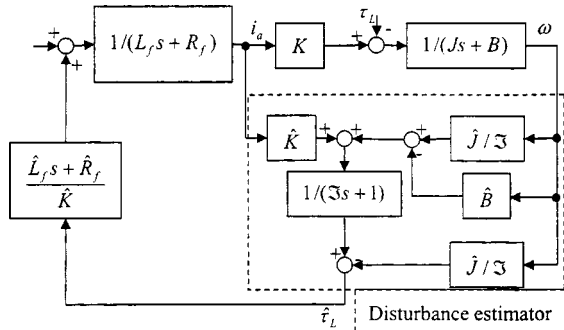The electronic gearing (E-gearing) differentiates itself from the mechanical gearing because the

Fig. 3. The external disturbance estimator and external disturbance eliminated control. (i) $k \leq N+1$, $\omega_0 \sim \omega_{k-1}$ are the recorded data and $\hat{\omega}_k$ is the unknown (estimated) data. (ii) $k > N+1$, $\omega_{k-N-2} \sim \omega_{k-1}$ are the recorded data and $\hat{\omega}_k$ is the unknown (estimated) data.

E-gearing system employs only electronic means to achieve the constant input/output velocity ratio. It is assumed that the output velocity control system is stiff and the main issue for the electronic E-gearing is to predict the future master velocity from its past. The velocity of the slave (output) motor is controlled according to the velocity of the master (input) motor.

The velocity of the master motor varies when loads or other external disturbances are applied. Therefore the master velocity is not usually constant and may exhibit harmonics. Even though the amplitudes of the harmonic velocity are greatly reduced by using the proposed disturbance estimator, there still exists velocity variations. The procedure for estimating the master position and/or velocity is an important step for E-gearing. Methods of tracking control have been developed in various fields, and include radar tracking control and others [12]. This study proposes an Nth-order polynomial tracking method to perform the E-gearing process.

According to the Nth-order polynomial, the master velocity at time t can be expressed as

$$\omega = \sum_{i=0}^{N} c_i t^i. \qquad (4)$$

To determine the above coefficients $(c_0, c_1, \ldots, c_N)$ in real time, two procedures are proposed.

(i) The initial procedure, $t = kT$, $1 \leq k \leq N+1$, is the various order $[(k-1)$th order$]$ polynomial extrapolation, where the symbol k is a real-time counter of time base, T is the PC-based programming sampling time, and kT denotes the present time over all this paper,

(I) $k \leq N+1$, $\omega_0 \sim \omega_{k-1}$ are the recorded data and $\hat{\omega}_k$ is the unknown (estimated) data.

(II) $k > N+1$, $\omega_{k-N-2} \sim \omega_{k-1}$ are the recorded data and $\hat{\omega}_k$ is the unknown (estimated) data.
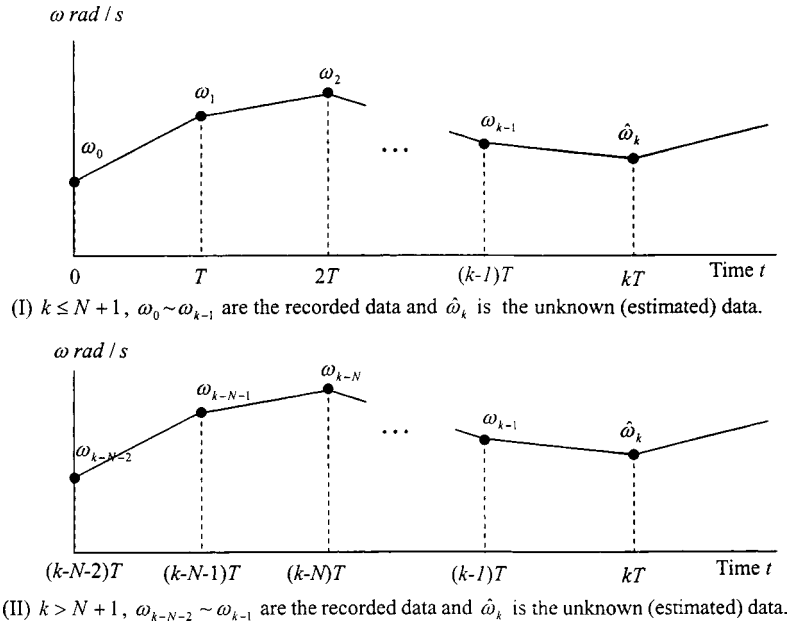
Fig. 4. Temporal relations between the two proposed procedures.

$$\sum_{i=0}^{k-1} c_i(l \cdot T)^i = \omega_l, \quad l=0 \text{ to } k-1. \quad (5)$$

Here we use the assumption of $0^0 = 1$.

(ii) The main procedure, $t = kT$, $k > N+1$, is the fixed Nth-order polynomial extrapolation:

$$\sum_{i=0}^{N} c_i(j \cdot T)^i = \omega_l, \quad l=(k-N-1) \text{ to } (k-1),$$

$$j = l - (k-N-1). \quad (6)$$

Similarly, the symbol k is a real-time counter of time base, T is the PC-based programming sampling time. Where $\omega_l[= (x_{l+1} - x_l)/T]$ are the measured angular velocities during the interval $[lT,(l+1)T]$, x_l are the recorded positions of the master measured from the encoder at the past time lT. Furthermore, Fig. 4 shows the temporal relations of the two proposed procedures.

Rewriting Eq. (6) in matrix form yields

$$\mathbf{M} \cdot \mathbf{C}_k = \mathbf{\Omega} \Rightarrow \mathbf{C}_k = \mathbf{M}^{-1} \cdot \mathbf{\Omega}, \quad (7)$$

where $\mathbf{M} \in \mathbf{R}^{(N+1) \times (N+1)}$, $\mathbf{C}_k \in \mathbf{R}^{N+1}$, and $\mathbf{\Omega}$ are the obtained time matrix, the matrix of polynomial coefficients, and the matrix of measured angular velocities, respectively. Moreover, the element of $\mathbf{M}$ in the ith row and jth column can be expressed as

$$m_{i,j} = [(i-1)T]^{j-1}, \quad (8)$$

$$\mathbf{C}_k = [c_0, c_1, \ldots, c_N]^T,$$

$$\mathbf{\Omega} = [\omega_{k-N-1}, \omega_{k-N}, \ldots, \omega_{k-1}]^T. \quad (9)$$

In Eq. (8), $\mathbf{M}$ is a constant matrix and $\mathbf{M}^{-1}$ exists; the computation involves no numerical degeneracy. Then the estimated velocity $\hat{\omega}_k$ during the time interval $[kT,(k+1)T]$ can be calculated as

$$\hat{\omega}_k = [1, NT, \ldots, (NT)^{N-1}] \cdot \mathbf{C}_k. \quad (10)$$

However, the estimated initial angular velocity may be chosen as the reference master velocity $\bar{\omega}$ which is the desired velocity of the master, i.e., $\hat{\omega}_0 = \bar{\omega}$. Then, the estimated position of the master is

$$\hat{x}_{k+1} = x_k + \hat{\omega}_k \cdot T, \quad (11)$$

where x_k and $\hat{x}_{k+1}$ are the measured position of the master at the present sample time kT and the estimated position at the next sample time $(k+1)T$, respectively.

Table 1
An example of cam profile table, both sets of data are scaled by their largest travel distance of one cam cycle.

Master position x	0	0.1	0.2	0.3	0.4	0.5	0.6	0.7	0.8	0.9	1
Slave position $f(x)$	0	0.006 45	0.048 63	0.148 63	0.306 45	0.5	0.693 55	0.851 37	0.951 37	0.993 55	1

4. Predicting the position of the slaves

This study uses Lagrange's interpolation formula to establish piecewise cam trajectories. If the piecewise reciprocal master-slave's coordinates (x_i, y_i) obtained from the given cam profile table specify $n+1$ points, where $i=0$ to n, and $x_0 < x_1 < \cdots < x_n$, then the nth-degree Lagrange polynomial is

$$f_L(x) = \sum_{i=0}^{n} L_i(x) y_i, \qquad (12)$$

where

$$L_i(x) = \prod_{j=0, j \neq i}^{n} \left(\frac{x - x_j}{x_i - x_j} \right) \qquad (13)$$

are the Lagrange interpolation coefficients. Table 1 is an example of a cam profile table.

Substituting Eq. (11) into Eq. (12) yields the next ideal cam profile position of the slave:

$$f_L(\hat{x}_{k+1}) = \sum_{i=0}^{n} L_i(\hat{x}_{k+1}) y_i. \qquad (14)$$

The design of the cam profile may not consider the dynamic capability of the control plant in advance. Some dynamic limitations that degrade the slave motion generally apply; for example, a cutting machine tool may chatter due to over-large jerk, so the jerk has to be limited during the cutting process. Furthermore, maximal velocity and acceleration are limited by the motor and servo drive system. Consequently, the actual trajectory of slave motion may not be fulfilled, Eq. (14), but must be close to the ideal trajectory provided that it fits the specified constraints. Given its low sensitivity, the piecewise trajectory of the actual slave motion with respect to time is proposed to follow a cubic B-spline curve of fourth degree [9], as shown in Fig. 5:

$$r_{k+1,j}(u) = F_{1,4}(u) p_{k+1,j-1} + F_{2,4}(u) p_{k+1,j}$$
$$+ F_{3,4}(u) p_{k+1,j+1} + F_{4,4}(u) p_{k+1,j+2},$$
$$\qquad (15)$$

where $r_{k+1,j}(u)$ represents the jth segment of the $(k+1)$th time interval; $j \in [1:4]$ denotes the curve segment number and $u=0$ to 1 within each curve segment. $p_{k+1,j-1} \sim p_{k+1,j+2}$ are the control points of the spline. $F_{1,4}(u) \sim F_{4,4}(u)$ are the blending functions.

The fourth degree cubic B-spline, as shown in Fig. 8, exhibits second-order continuity. All the variables of the B-spline are defined below.

(i) $p_{k+1,0}(=p_{k-4,5})$ denotes the initial control point of the $(k+1)$th time interval, where $p_{k-4,5}$ is the previous position command of the slave at time $(k-4)T$ and equivalently the fifth control point of the $(k-4)$th time interval.

(ii) $p_{k+1,1}(=p_{k-3,5})$ denotes the first control point of the $(k+1)$th time interval, where $p_{k-3,5}$ is the previous position of the slave at time $(k-3)T$ and equivalently the fifth control point of the $(k-3)$th time interval.

(iii) $p_{k+1,2}(=p_{k-2,5})$ denotes the second control point of the $(k+1)$th time interval, where $p_{k-2,5}$ is the previous position of the slave at time $(k-2)T$ and equivalently the fifth control point of the $(k-2)$th time interval.

(iv) $p_{k+1,3}(=p_{k-1,5})$ denotes the third control point of the $(k+1)$th time interval, where $p_{k-1,5}$ is the previous position of the slave at time $(k-1)T$ and equivalently the fifth control point of the $(k-1)$th time interval.

(v) $p_{k+1,4}(=p_{k,5})$ denotes the fourth control point of the $(k+1)$th time interval, where $p_{k,5}$ is the previous position of the slave at time kT and equivalently the fifth control point of the kth time interval.

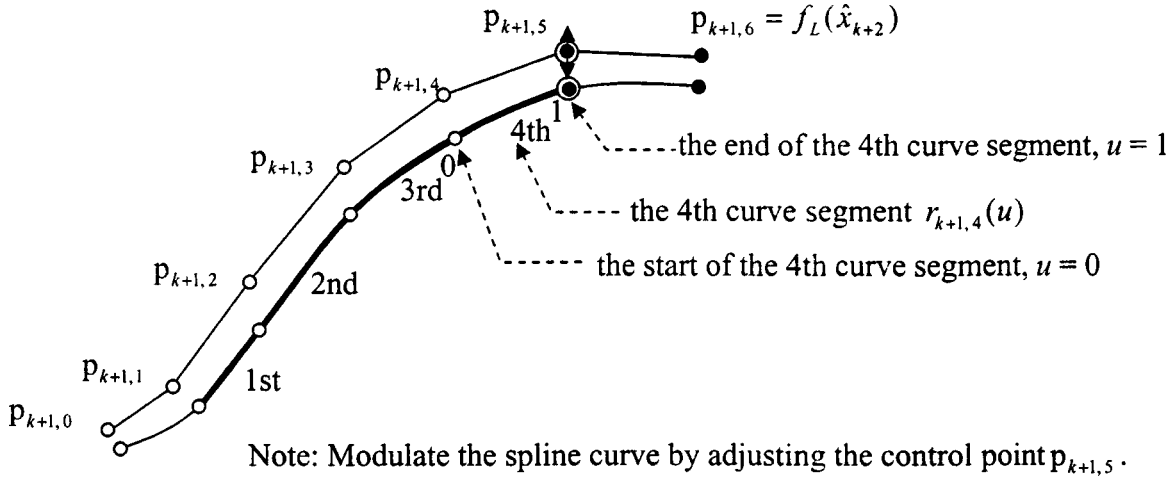(vi) $p_{k+1,5}$ denotes the position command of the slave motor yet to be determined, and is equiva-

Fig. 5. $r_{k+1,j}(u)$, and its control points, $p_{k+1,0} \sim p_{k+1,6}$.

lently the fifth control point of the $(k+1)$th time interval.

(vii) $p_{k+1,6}[=f_L(\hat{x}_{k+2})]$ denotes the sixth control point of the $(k+1)$th time interval, where $f_L(\hat{x}_{k+2})$ is derived from the cam profile position at time $(k+2)T$, as indicated in Eq. (14).

Statements (i)–(vii) include a total of seven unknowns and six independent equalities. There is an extra degree of freedom left for the following optimization problem: The slave's position error between the next unknown position command $p_{k+1,5}$ and the ideal cam profile position command $f_L(\hat{x}_{k+1})$ at time $(k+1)T$ can be expressed as

$$e_{k+1} = p_{k+1,5} - f_L(\hat{x}_{k+1}). \qquad (16)$$

The objective error function is defined in quadratic form as

$$E_{k+1} = \|e_{k+1}\|_2^2 = \|p_{k+1,5} - f(\hat{x}_{k+1})\|_2^2. \quad (17)$$

To ensure that the velocity, acceleration, and jerk do not exceed the maximal values, ($V_{\max}$, $A_{\max}$, and $\text{Jerk}_{\max}$) allowed for the motor's system, three inequality constraints are imposed on the optimization. The first, second, and third differentiation of the cubic B-spline curve at the start, $u=0$, of the fourth segment, can be expressed as follows:

$$r_{k+1,4}^u(0) = -0.5p_{k+1,3} + 0.5p_{k+1,5}, \quad (18a)$$

$$r_{k+1,4}^{uu}(0) = p_{k+1,3} - 2p_{k+1,4} + p_{k+1,5}, \qquad (18b)$$

$$r_{k+1,4}^{uuu}(0) = -p_{k+1,3} + 3p_{k+1,4} - 3p_{k+1,5} + p_{k+1,6}. \qquad (18c)$$

Minimizing the objective error function subject to the constraints on velocity, acceleration, and jerk yields the one-dimensional constrained optimization problem:

$$\text{Minimize } \|p_{k+1,5} - f(\hat{x}_{k+1})\|_2^2 \qquad (19a)$$

$$\text{subject to } \begin{cases} |r_{k+1,4}^u(0)| \le V_{\max} & (19b) \\ |r_{k+1,4}^{uu}(0)| \le A_{\max} & (19c) \\ |r_{k+1,4}^{uuu}(0)| \le \text{Jerk}_{\max}. & (19d) \end{cases}$$

The constrained optimization problem of a quadratic cost function has an easy to find optimal solution, $p_{k+1,5}^* = f_L(\hat{x}_{k+1})$ with zero cost, when none of the constraints is violated. According to Eqs. (19a)–(19d), the optimization problem may be reformulated as an unconstrained minimization problem as follows:

$$\text{Minimize } \|p_{k+1,5} - f(\hat{x}_{k+1})\|_2^2 + W_v g_v(p_{k+1,5})$$
$$+ W_a g_a(p_{k+1,5}) + W_J g_J(p_{k+1,5}), \qquad (20)$$

where W_v, W_a, and W_J are the weighting factors of velocity constraint, acceleration constraint, and jerk constraint, respectively, and
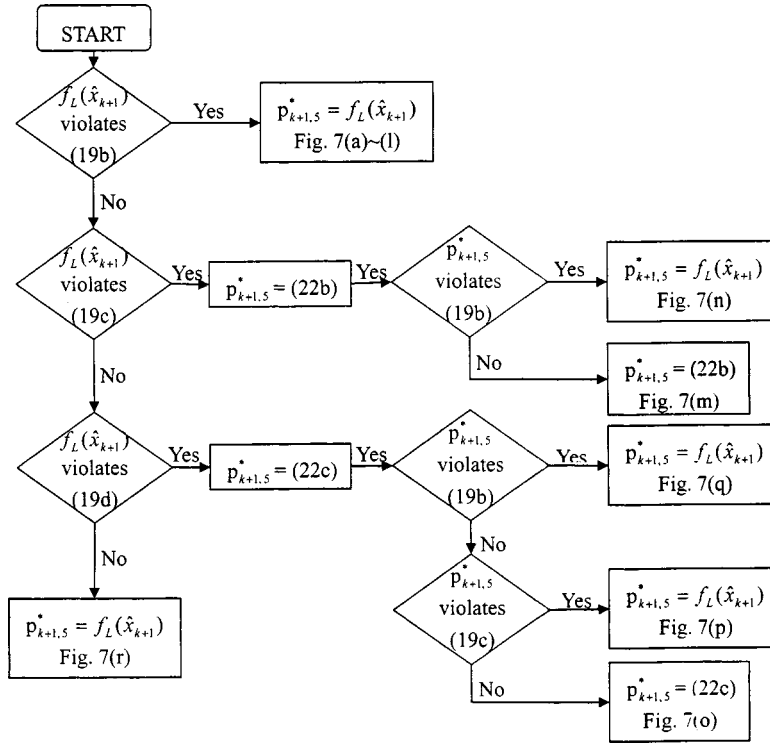
Fig. 6. Flow chart of the optimal solution process.

$$g_v(p_{k+1,5}) = \begin{cases} ||r^u_{k+1,4}(0)| - V_{\max}|, \\ \quad \text{if } |r^u_{k+1,4}(0)| < V_{\max} \\ 0, \quad \text{if } |r^u_{k+1,4}(0)| \geq V_{\max}, \end{cases}$$
(21a)

$$g_a(p_{k+1,5}) = \begin{cases} ||r^{uu}_{k+1,4}(0)| - A_{\max}|, \\ \quad \text{if } |r^{uu}_{k+1,4}(0)| < A_{\max} \\ 0, \quad \text{if } |r^{uu}_{k+1,4}(0)| \geq A_{\max}, \end{cases}$$
(21b)

$$g_J(p_{k+1,5}) = \begin{cases} ||r^u_{k+1,4}(0)| - \text{Jerk}_{\max}|, \\ \quad \text{if } |r^{uuu}_{k+1,4}(0)| < \text{Jerk}_{\max} \\ 0, \quad \text{if } |r^{uuu}_{k+1,4}(0)| \geq \text{Jerk}_{\max}. \end{cases}$$
(21c)

In an extreme case that $W_v \gg W_a \gg W_J$, the minimization problem implies a constraint violation priority that g_v is much more important than g_a and g_J. In practice, Eq. (19) is highly nonlinear, existing techniques to find the global optimization are not guaranteed. One needs to enumerate all the possible cases for the global solution. Fig. 7 shows all the possible optimal solution for the extreme

case that $W_v \gg W_a \gg W_J$. The bounds of $p_{k+1,5}$ for each of the constraints may be easily calculated from Eqs. (19b)–(19d) by substituting the inequality sign into equality sign, as follows:

$$p_{k+1,5} = 2 \, \text{sgn}[r^u_{k+1,4}(0)] \cdot V_{\max} + p_{k+1,3},$$
(22a)

$$p_{k+1,5} = \text{sgn}[r^{uu}_{k+1,4}(0)] \cdot A_{\max} - p_{k+1,3} + 2p_{k+1,4},$$
(22b)

$$p_{k+1,5} = -\tfrac{1}{3} \text{sgn}[r^{uuu}_{k+1,4}(0)]\text{Jerk}_{\max} - \tfrac{1}{3} p_{k+1,3}$$
$$+ p_{k+1,4} + \tfrac{1}{3} p_{k+1,6}.$$
(22c)

The optimal solution process may be depicted in the flow chart as shown in Fig. 6. According to the flow chart, the solution of the optimization problem is unique, and thus guarantees to be the global optimum.

In Fig. 6, all possible cases are enumerated and categorized as follows. (i) The ideal cam profile position command violates the velocity constraint, as shown in Figs. 7(a)–7(l); (ii) the ideal cam profile position command violates acceleration constraint and does not violate velocity constraint, as
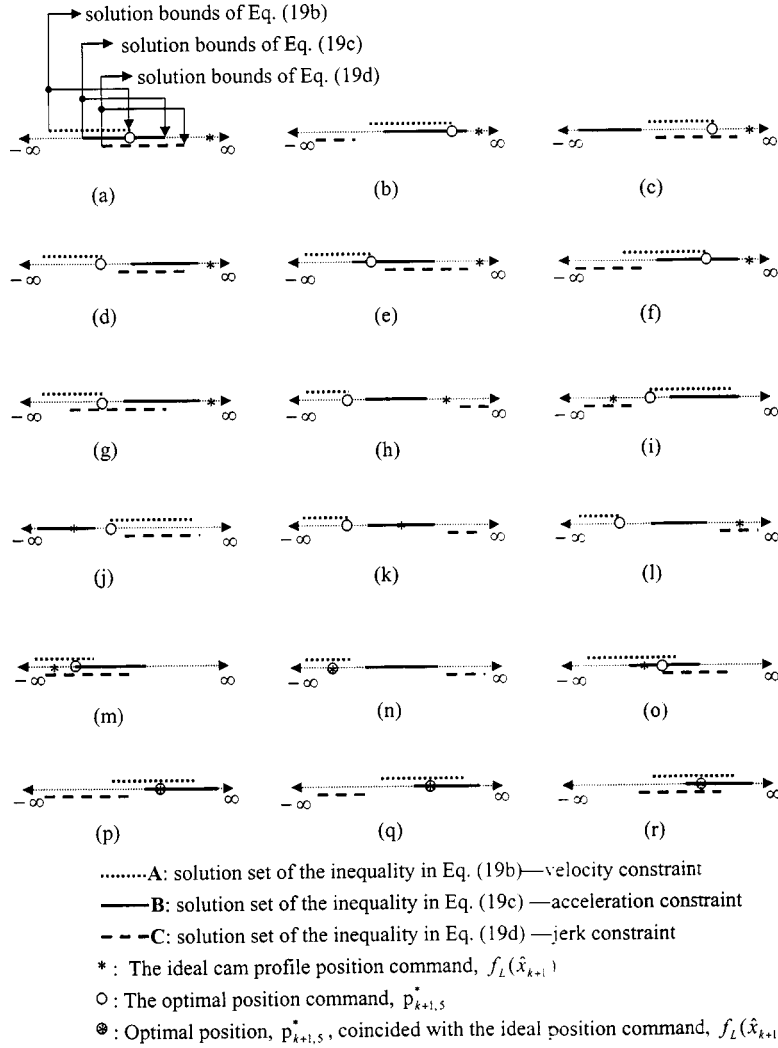
solution bounds of Eq. (19b)
solution bounds of Eq. (19c)
solution bounds of Eq. (19d)

(a)   (b)   (c)

(d)   (e)   (f)

(g)   (h)   (i)

(j)   (k)   (l)

(m)   (n)   (o)

(p)   (q)   (r)

········ **A**: solution set of the inequality in Eq. (19b)—velocity constraint
——— **B**: solution set of the inequality in Eq. (19c) —acceleration constraint
– – –**C**: solution set of the inequality in Eq. (19d) —jerk constraint
* : The ideal cam profile position command, $f_L(\hat{x}_{k+1})$
○ : The optimal position command, $p^{\bullet}_{k+1,5}$
⊕ : Optimal position, $p^{\bullet}_{k+1,5}$, coincided with the ideal position command, $f_L(\hat{x}_{k+1})$

Note: The above categories are in the extreme case that $W_v \gg W_a \gg W_J$

Fig. 7. The location of the optimal position command, $p^*_{k+1,5}$, for all different cases.

shown in Figs. 7(m) and 7(n); (iii) the ideal cam profile position command violates only the jerk constraint, as shown in Figs. 7(o)–7(q); (iv) the ideal cam profile position command satisfies all of the constraints, as shown in Fig. 7(r).

5. Simulation and experimental results

5.1. Simulation of disturbance estimator

For simulation purposes, the nominal external disturbance is assumed to be a square wave function:

$$\tau_L = \underline{\quad\quad\quad} \quad (23)$$

The amplitude a of the square wave is set to 4.8773 N m and the frequency of the square wave is 1 Hz. Figs. 8(a) and 8(b) present the master's simulated angular velocity obtained using the proposed disturbance estimator feedback control and without using the disturbance estimator. The nominal parameters of the master motor defined in Section 2 are $\hat{K} = 0.55\,\mathrm{N\,m/A}$, $\hat{J} = 0.093\,\mathrm{kg\,m^2}$,
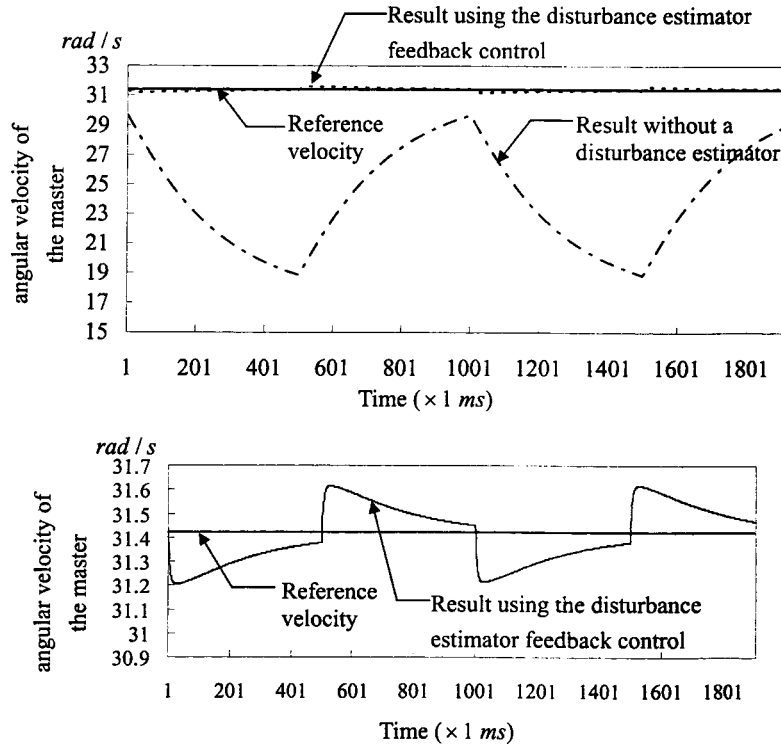
Fig. 8. (a) Simulated angular velocity of the master. (b) Simulated angular velocity of the master using disturbance estimator feedback control (zoom in).
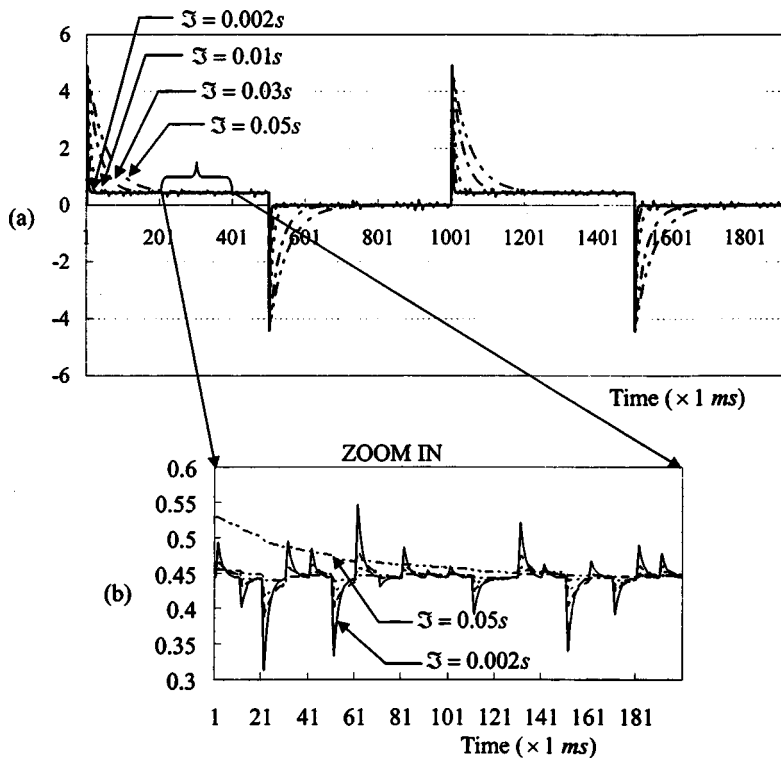

Fig. 9. The errors between the fed torque (τ_L) and the estimated torque ($\hat{\tau}_L$) with respect to various time constants $\Im$.

Table 2
Experimental specifications of parameters for the ECAM control, last four data are scaled by their largest travel distance of one cam cycle.

PC-based program-ming sampling time T	Polyno-mial order N	Critical slave velocity (C_v)	Critical slave accelera-tion (C_a)	Critical slave jerk (C_j)
0.01 s	0~5	1	10	600

$\hat{B} = 0.008$ N m s/rad, $L_f = 0.046$ H, $R_f = 1$ Ω, and $K_a = 0.55$ V s/rad. The sampling time of the current loop is set to 0.001 s in the simulation. Furthermore, the amplitude of the disturbance load torque is 4.8773 N m and the torque constant is 0.55 N m/A, that is, the operating current is about 8.9 A, the $i_a^2 R_f$ power loss is around 78.6 W (calculated by the paper reviewer). The power loss of 78.6 W in this case is not serious for the applications with motors up to several kW.
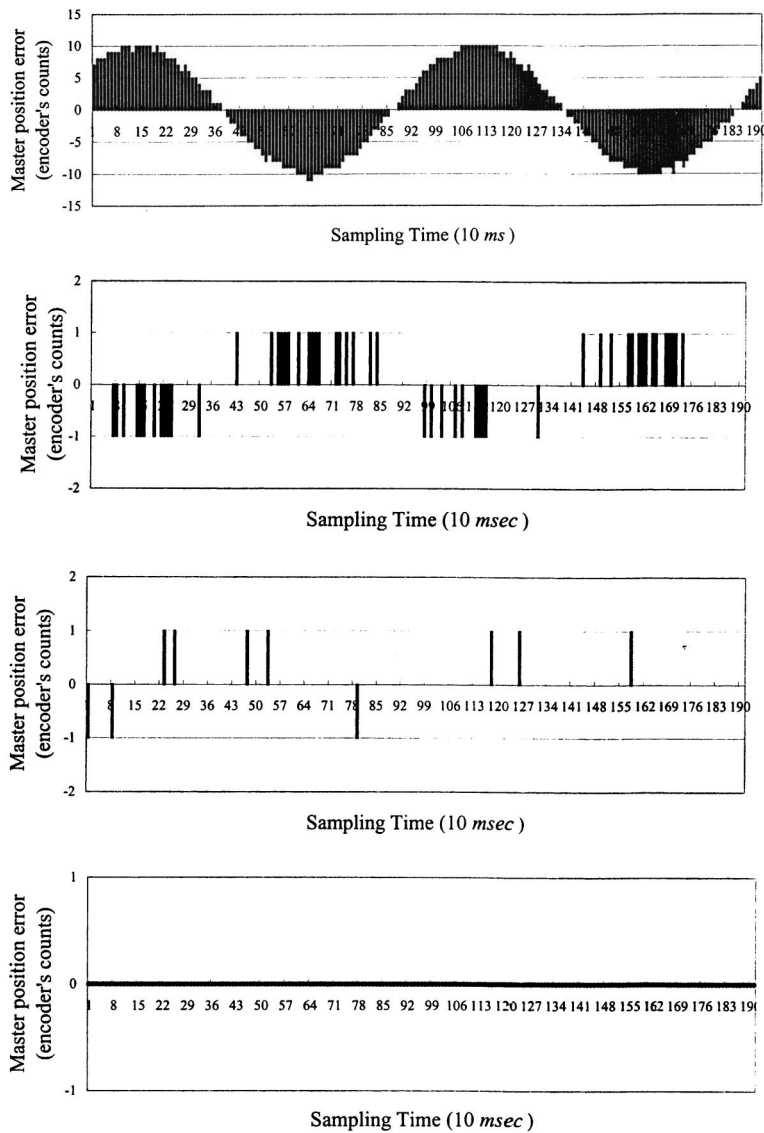

Fig. 10. (a) The tracking error of the master's position for the zero-order interpolation method. (b) The tracking error of the master for the third-order polynomial tracking method. (c) The tracking error of the master for the fourth-order polynomial tracking method. (d) The tracking error of the master for the fifth-order polynomial tracking method.

Table 3
The maximum tracking error of the master's position for the Nth-order polynomial tracking control ($N=0-5$).

Order	0th	1st	2nd	3rd	4th	5th
Max. err. (counts/20π rad)	11	17	3	1	1	0

Figs. 9(a) and 9(b) show the maximum errors between the fed torque τ_L and the estimated torque $\hat{\tau}_L$ for various time constants ($\Im$). In Fig. 9(a), a smaller $\Im$ yields a smaller mean torque error. However, Fig. 9(b) reveals that a lower $\Im$ yields a larger measurement noise. Furthermore, the measurement noise was assumed to be a zero-mean, normally (Gaussian) distributed random signal in the simulation.

Both a larger mean torque error and a larger measurement noise reduce the tracking performance of the master, so the time constant must be neither too small nor too large. In the experiment, the time constant $\Im$ of the disturbance estimator was set to ten times the current loop sampling time. As depicted in Fig. 8(b), the time constant $\Im$ and the current loop sampling time are set to 0.01 s and 0.001 s, respectively.

5.2. Experimental results for tracking performance of the electronic gearing process

Table 2 lists the parameter settings of the ECAM control. The accuracy of the tracking of the master's velocity is characterized by the maximum error between the actual position and the estimated position. Figs. 10(a)–(d) show that the maximum tracking error of the master's position, using the fifth-order polynomial tracking control method, is zero when the master's nominal mean speed is 10π rad/s. Table 3 shows the maximum tracking error of the master's position for polynomial tracking control methods of various orders ($N=0-5$).

5.3. Performance of the electronic cam process

Fig. 11(b) shows an example of a reference trajectory that corresponds to the electronic cam motion. According to a constant master speed of 10π rad/s and a maximum slave travel distance of 200π rad, the reference trajectory yields a 200π rad/s maximum slave speed, 1260π rad/s^2 maximum acceleration and 8120π rad/s^3 maximum
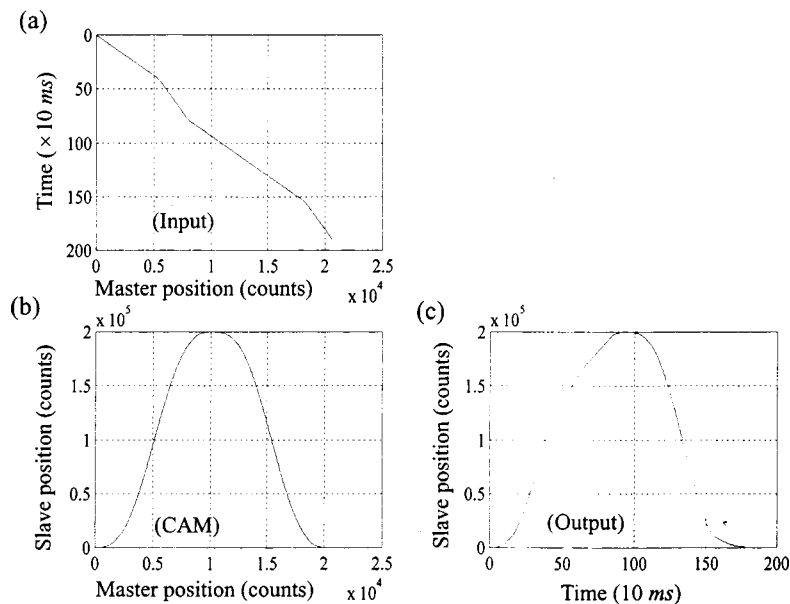

Fig. 11. The piecewise tracking trajectory of the electronic cam motion: (a) the actual master's position in real-time; (b) the reference trajectory corresponding to the electronic cam motion; (c) the actual cam trajectory in real-time. Note that the unit "counts" means the encoder's pulse counts and the resolution of the encoder is 2000 counts/revolution.
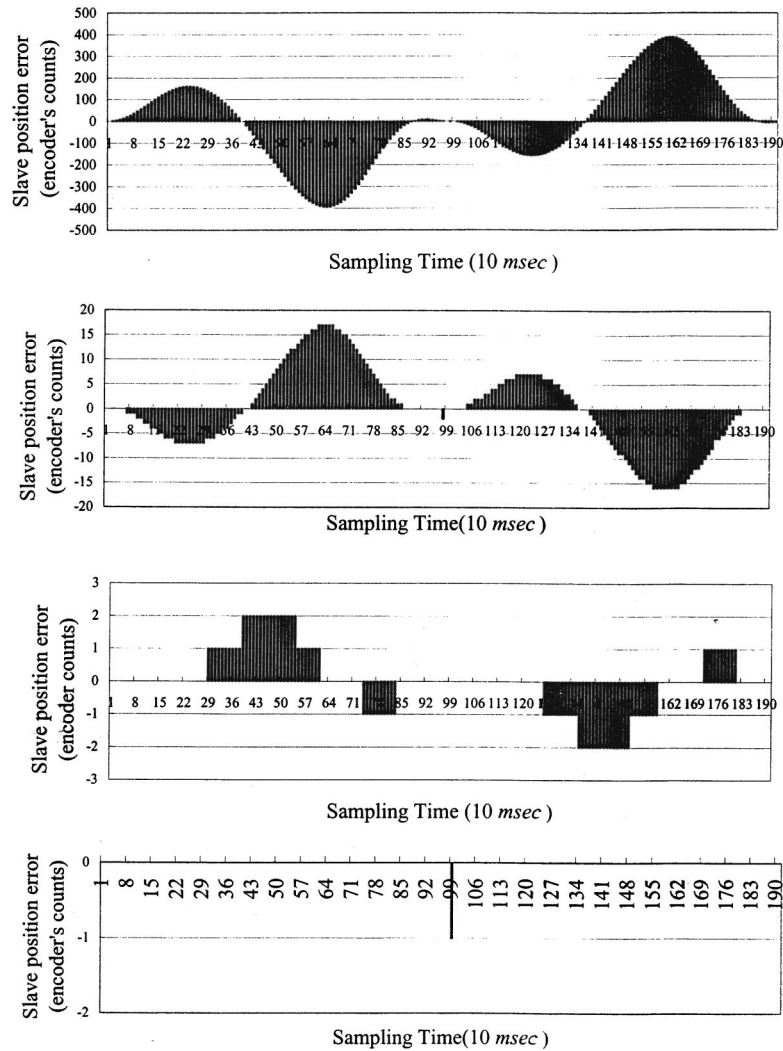
Fig. 12. (a) Cam profile error with the zero-order (conventional) tracking method (the maximum travel distance: 200 000 encoder's counts). (b) Cam profile error with the third-order polynomial tracking method (the maximum travel distance: 200 000 encoder's counts). (c) Cam profile error with the fourth-order polynomial tracking method (the maximum travel distance: 200 000 encoder's counts). (d) Cam profile error with the fifth-order polynomial tracking method (the maximum travel distance: 200 000 encoder's counts).

Table 4
An experimental example for the maximum tracking errors of the slave's position in the encoder's counts for the Nth-order polynomial master tracking control, the maximum travel distance is 200 000 encoder's counts (equivalent to 200π rad).

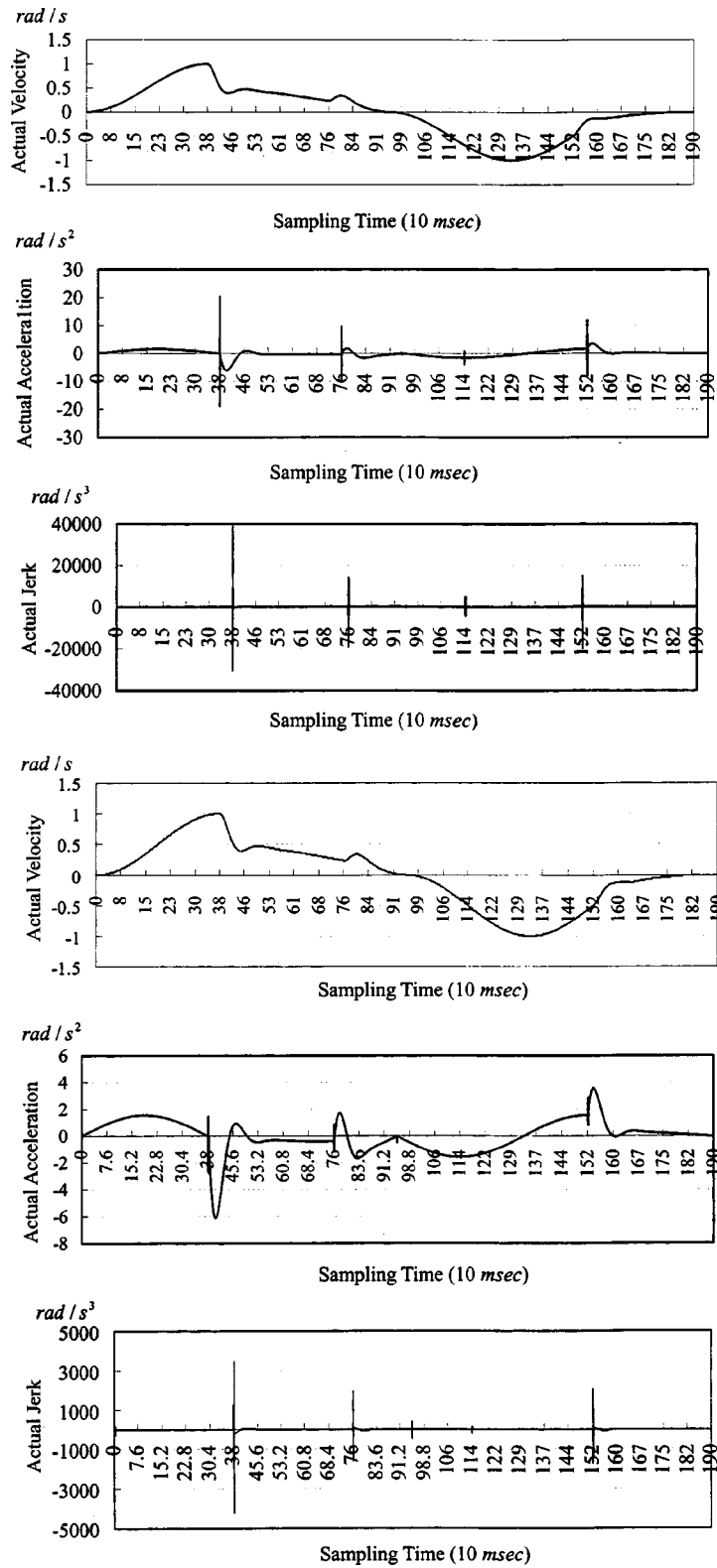| Order	0th	1st	2nd	3rd	4th	5th
Max. error (encoder's counts)	395	655	83	17	2	1
rms error	194.9368	325.6317	45.2338	8.1915	0.9681	0.144 715
Cycle-to-cycle variation	0.590 083	0.449 440	0.140 121	0.075 427	0.129 316	0.072 357

Fig. 13. (a) The tracking result of the slave velocity, acceleration, and jerk purely based on the Lagrange polynomial curve-fitting with no optimization. (b) The result of the slave velocity, acceleration, and jerk applying the optimization.

Table 5
An experimental example for the maximum slave velocity, acceleration, and jerk based purely on the Lagrange polynomial curve-fitting and applying the optimization algorithm to the cubic B-spline curve-fitting process.

Performance index conditions	Maximum velocity	Maximum acceleration	Maximum jerk
Applying the optimization algorithm to the cubic B-spline curve-fitting process	1 (scaled) (equivalent to 628.32 rad/s)	6.1422 (scaled) (equivalent to 3859 rad/s^2)	572.2694 (scaled) (equivalent to 3.59e05 rad/s^3)
Purely curve-fitting using Lagrange polynomial	1 (scaled) (equivalent to 628.32 rad/s)	20.12 (scaled) (equivalent to 12644 rad/s^2)	3980.95 (scaled) (equivalent to 2.50e06 rad/s^3)

jerk. The master's speed is generally not constant and may be harmonic, as shown in Fig. 7. The speed will exhibit the actual position of the master and the ideal cam trajectory, as shown in Figs. 11(a) and 11(c), respectively. This piecewise cam trajectory contains 191 points. Three performance indices are used to quantify the accuracy and consistency. The tracking accuracy of the slave motion is characterized by the maximum error and the root-mean-square (rms) error. The consistency of the cam tracking—that is, the cycle-to-cycle variation—is characterized by the rms difference between the particular error response and the error response averaged over a number of cycles. Fifty cycles of tracking error data were collected. Figs. 12(a)–12(d) summarize the results of slave position. Table 4 lists the maximum tracking errors of the slave's position in encoder counts, using the Nth-order polynomial tracking control method and the pure Lagrange polynomial curve-fitting method. Furthermore, Fig. 13 shows the partial results of the slave's tracking velocity, acceleration, and jerk, according to Lagrange polynomial curve-fitting with or without the aforementioned optimization. Similarly, Table 5 indicates the tracking control performance, also for the Lagrange polynomial curve-fitting method with or without the aforementioned optimization.

5.4. Computational load on the CPU of the proposed ECAM tracking control

The selection of N depends on the accuracy demanded. As stated above, tracking using a higher-order polynomial yields higher precision; however, a tradeoff exists between the "order" of the polynomial used and the CPU time required. In
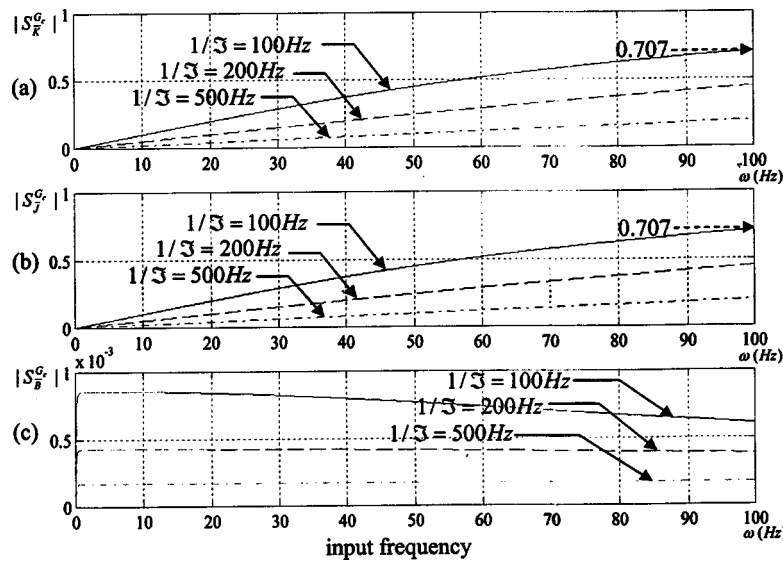

Fig. 14. Magnitudes of the sensitivities: (a) $S_K^{G_c}$, (b) $S_J^{G_c}$, and (c) $S_B^{G_c}$, in relation to the input frequency ω at various time constants $\Im$.

practice, the computational time of the proposed algorithm (fifth-order tracking) is about 0.02 ms in a programming cycle on an Intel Pentium III 900-MHz CPU. The computational time of a programming cycle is much less than the PC-based sampling time, 10 ms.

6. Conclusion

The proposed disturbance estimator can effectively suppress the external disturbance and the high-frequency measurement noise, trading off delay time and the robustness of the estimator. As a result, higher-order polynomial fitting must be adapted for a cam profile with a farther travel distance. The cam profile tracking is formulated as optimization in real-time control. A deterministic and unique solution is derived for all possible cases of tracking control. The proposed method is effective for general motion tracking control and guarantees a global optimal solution for practical control.

Acknowledgment

Appendix

The physical parameters of the motor may be dynamically varied, so the effect of parameter uncertainty must also be discussed. The well-known analysis of the modeling uncertainty is the μ analysis [13]. A more direct method is to analyze the sensitivities ($S_{\bar{K}}^{G_c}$, $S_{\bar{J}}^{G_c}$, and $S_{\bar{B}}^{G_c}$) of the transfer function G_c to the motor's uncertain parameters, $\bar{K}$, $\bar{J}$, and $\bar{B}$, respectively, where

$$G_c = \frac{K\bar{K}(\Im s + 1)}{K\bar{J}\Im s^2 + (K\bar{B}\Im + \bar{K}J)s + \bar{K}B}, \quad \text{(A1)}$$

$$S_{\bar{K}}^{G_c} = \frac{\partial G_c}{\partial \bar{K}} \cdot \frac{\bar{K}}{G_c} = \frac{K\bar{J}\Im s^2 + K\bar{B}\Im s}{K\bar{J}\Im s^2 + (K\bar{B}\Im + \bar{K}J)s + \bar{K}B}, \quad \text{(A2)}$$

$$S_{\bar{J}}^{G_c} = \frac{\partial G_c}{\partial \bar{K}} \cdot \frac{\bar{K}}{G_c} = \frac{-K\bar{J}\Im s^2}{K\bar{J}\Im s^2 + (K\bar{B}\Im + \bar{K}J)s + \bar{K}B}, \quad \text{(A3)}$$

$$S_{\bar{B}}^{G_c} = \frac{\partial G_c}{\partial \bar{K}} \cdot \frac{\bar{K}}{G_c} = \frac{-K\bar{B}\Im s^2}{K\bar{J}\Im s^2 + (K\bar{B}\Im + \bar{K}J)s + \bar{K}B}. \quad \text{(A4)}$$

Figs. 14(a)–14(c) show the magnitudes of the three sensitivities in relation to the input frequency, where the parameters of the master motor are all set as in Section 5. According to Eqs. (A2) and (A3), the magnitudes of the sensitivities, $S_{\bar{K}}^{G_c}$ and $S_{\bar{J}}^{G_c}$, are both small for low-frequency motion. Figs. 14(a) and 14(b) reveal that the magnitudes of the sensitivities, $S_{\bar{K}}^{G_c}$ and $S_{\bar{J}}^{G_c}$, are both less than 0.707 while the input frequency is lower than $1/\Im$ Hz. Furthermore, according to Fig. 14(c), the magnitude of the sensitivity $S_{\bar{B}}^{G_c}$ is less than 0.000 86 over the entire frequency domain. From Eqs. (A1)–(A3) and the foregoing discussion, the low time constant $\Im$ of the disturbance estimator suppresses the sensitivities, $S_{\bar{K}}^{G_c}$, $S_{\bar{J}}^{G_c}$, and $S_{\bar{B}}^{G_c}$.

References

[1] Steven, Chingyei Chung, Tracking Control for the Electric Gear System. National Science Council of the Republic of China 845-012-011, 1995, pp. 1–35.

[2] Zhao, Qing-Feng, Advanced Design for Automatic Control System. Chan Hwa Science and Technology Book Co., 2000, Chap. 4, pp. 1–26.

[3] Gavrilovic, A. and Heath, A. J., Prediction and Mitigation of System Disturbances to Industrial Loads, Sources and Effects of Power System Disturbances. IEE Conference publication, 1982, pp. 227–230.

[4] Phillips, Charles L. and Nagle, H. Troy, Digital Control System Analysis and Design. Prentice-Hall International Editions, NJ, 1994, pp. 103–144.

[5] Yan, H. S., Tsai, M. C., and Hsu, M. H., An experimental study of the effects of cam speed on cam-follower systems. Mech. Mach. Theory **31**, 397–412 (1996).

[6] Yan, H. S., Tsai, M. C., and Hsu, M. H., A variable-speed method for improving motion characteristics of cam-following system. J. Mech. Des. **118**, 250–258 (1996).

[7] Chen, Li-Shan, Follower Motion Design in a Variable-Speed Cam System. Master thesis, Institute of Mechanical Engineering College of Engineering, National Chiao Tung University, 1995, pp. 1–49.

[8] Dierchx, Paul, Curve and Surface Fitting with Splines. Oxford University Press, New York, 1993, pp. 75–91.

[9] Mortenson, Michael E., Geometric Modeling. John

Wiley & Sons, Inc., New York, 1985, pp. 91–146.

[10] Kim, Dean H. and Tsao, Tsu-Chin, Robust performance control of electrohydraulic actuators for electronic cam motion generation. IEEE Trans. Control Syst. Technol., **8**, 220–227 (2000).

[11] Chong, Edwin K. P. and Żak, Stanislaw H., An Introduction to Optimization. John Wiley & Sons, Inc., New York, 1996, pp. 101–164.

[12] Blackman, Samuel and Popoli, Robert, Design and Analysis of Modern Tracking Systems. Artech House-Publishers, Boston, 1999, pp. 147–195.

[13] Zhou, Kemin, Essentials of Robust Control. Prentice Hall, Inc., Upper Saddle River, NJ, 1998, pp. 55–62 and 129–211.

Shyr-Long Jeng received a Ph.D. in mechanical engineering at National Chiao-Tung University in 1996. He was appointed an assistant professor in automation engineering at Ta-Hwa Institute of Technology in 1998. From 1996 to 1998, he joined an electrical motor design company. His current research is in the microprocessor-based control and applications.

Chung-Shu Liao received the M.S. degree in mechanical engineering at National Chiao-Tung University in 1995. He has been a Ph.D. candidate in mechanical engineering at National Chiao-Tung University since 2000. From 1995 to 2000, he served as a high school teacher of mathematics. His current research is in the motion simulator system for entertainment games.

Wei-Hua Chieng received a Ph.D. in mechanical engineering at Columbia University in 1989. He has been a full professor in mechanical engineering at National Chiao-Tung University since 1996 and was appointed associated professor in 1989. His current research is in PC based control.